Wireless Communication Systems With Spatial Diversity: A Volumetric Model

Leif Hanlen, *Member, IEEE*, and Minyue Fu, *Fellow, IEEE*

***Abstract*—This paper presents a novel physical-modeling approach to wireless systems with multiple antennas. The fundamental problem of modeling the communication channel is studied, where the channel consists of a finite spatial volume for transmitting, a finite spatial volume for reception, and an arbitrary set of reflective-scattering bodies. The number of communication modes (or degrees of freedom) for such a system is calculated, using the procedure developed. We present a simple model for multipath channels, which allows insight into the development of a correlated multiple-input multiple-output (MIMO) channel model. In particular, the model is independent of transmitter and receiver elements and relies on the physical parameters of the channel involved. Our work explains which physical parameters determine the channel model and its channel capacity.**

***Index Terms*—Information rates, multipath channels, multiple-input multiple-output (MIMO) systems.**

I. Introduction

MULTIPATH has been shown to improve capacity in wireless communications under the assumption that the channel model is a random matrix with independent identically distributed (i.i.d.) elements [1], [2]. More specifically, the capacity of a multiantenna system with dense scattering has been shown to grow proportionally with the minimum of the numbers of transmitters and receivers [1], [2]. This is known as the linear-growth property of MIMO systems.

Much of the early work on MIMO wireless systems assumed that the channel model was a random matrix with i.i.d. element distribution [1], [2]. In [3], an experimental system was developed and tested for an indoor environment confirming the increase in channel capacity when multiple antennas are used. Recently several authors have addressed correlations in the fading environment [4], [5], antenna separation [6], and coupling between array elements [7]. A large amount of work has also focused on modeling of channels for multiantenna systems [8] and many authors have presented measurement campaigns addressing MIMO wireless channels. The diversity benefits of nonline-of-sight (NLOS) indoor channels have been investigated in the presence of dominant paths and polarization [9], and in outdoor environments [10]. In each case, greater or lesser improvements for channel capacity have been shown dependent upon the channel correlation. This leads to the natural question "Given an arbitrary volume, containing transmit elements, a second arbitrary volume containing receive elements and a group of scattering bodies, how many independent parallel channels are available?"

In order to address this question we must move away from standard point-defined multiple-antenna models to a functional-analysis viewpoint. The modeling of multiple-element arrays as collections of points is not appropriate for large numbers of closely placed elements: correlation matrices and mutual coupling hide the fact that antenna elements only sample a continuous spatial signal, in an analogous way to the sampling of a continuous-time signal. This has been examined in [11], where a random i.i.d. channel model was used, but the unbounded growth is rectified using a scaling parameter. It has been suggested that dense antenna arrays in the presence of scattering should also exhibit such a limit [12], however the authors' focus was on the coupling of antenna elements rather than an intrinsic capacity of the volume-to-volume communication channel. Some work has considered exploiting the coupling effects of antenna elements [13] for multiple-antenna arrays. The work of [7] and [14] has also addressed this concept. Coupled with the theoretical work of [15] these results suggest that there are fundamental physical limits to the capacity growth of a given MIMO channel, independent of the number of antenna elements.

We may view antenna elements as sampling functions, as given in [16], and consider space as a continuous parameter for input and output signals. We shall not address sampling in this paper; it would suffice to say that different arrangements of antenna elements correspond to different choices of sampling functions in the same way that continuous-time signals may be sampled at varying intervals. We provide a modeling technique that allows the examination of fundamental properties of the channel: we may consider correlation as an artifact of the use of antenna elements, rather than a property associated with spatial diversity. Consequently, once the volumetric approach is adopted, we may examine how to best utilize the channel in terms of the continuous spatial modes produced. The case without scattering bodies has been examined in [17] and its references for optical communications in free space. It is interesting that the setting in [17] is general and the results are equally applicable to radio communications.

Manuscript received November 1, 2002; revised December 1, 2004; accepted December 1, 2004. The editor coordinating the review of this paper and approving it for publication is H. Xu. A part of this paper was carried out while the authors visited Nanyang Technological University, Singapore. This paper appeared in part in IEEE International Conference on Communications, 2003 (ICC'03). A part of this work appeared in L. Hanlen's Ph.D. dissertation. National Information and Communications Technology (ICT) Australia is funded through the Australian Government's Backing Australia's Ability initiative, in part through the Australian Research Council.

L. Hanlen is with National Information and Communications Technology (ICT) Australia, Canberra, ACT 0200, Australia, and also with Australian National University, Canberra, ACT 0200, Australia (e-mail: leif.hanlen@nicta.com.au).

M. Fu is with the School of Electrical Engineering and Computer Science, University of Newcastle, Newcastle, NSW 2308, Australia.

Digital Object Identifier 10.1109/TWC.2005.858014

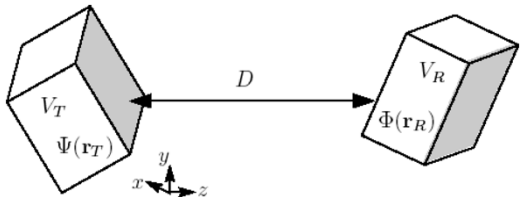

Fig. 1. Two-volume arrangement.

This paper provides a simple model for multipath scattering channels, which allows insight into the development of a volumetric MIMO channel model. In particular, we present a model that is independent of transmitter and receiver elements, and instead relies on the physical parameters of the channel involved. We show how to determine the number of communication modes (or degrees of freedom) for such a system.

This paper is arranged as follows. In Section II, we detail the wireless model for the two-body case (in free space) and provide a novel numerical approach in Section II-B for calculating the transfer-matrix elements for arbitrary bodies. In Section III, we generalize these results to include simple reflective-scattering bodies. In Section IV, examples are used to show how scattering bodies influence the channel model. We discuss the results in Section V and draw the conclusion in Section VI.

II. Modeling for Two-Volume Communications

Consider wireless communications between two arbitrary volumes as described in Fig. 1, where V_{T} is the transmitting body and V_{R} is the receiving body. The centers of the two bodies are separated by a distance D. It is assumed that the dimensions of the V_{T} and V_{R} are small compared to the distance D. We choose the coordinates (x, y, z) such that the z-axis is along the direction of D and the origin is the center of V_{T}. For simplicity, we consider single-frequency signals, and we assume that the channel is memoryless. The work in this paper may be generalized to the case where a finite frequency bandwidth is available.

Under the above constraints we may consider "signals" within V_{T} and V_{R} that are functions of space rather than time. The intuition of continuous-time channels [18, Ch. 8] may be applied with appropriate changes of variable. In particular, the channel between V_{T} and V_{R} may be represented in MIMO-matrix form using a matrix Γ. However, unlike standard wireless MIMO-matrix representations, where the matrix H represents channel gains between pointlike antenna elements, the matrix Γ represents channel gains between input signals and output signals that are functions defined over space. We may then consider exciting the channel with a particular choice of transmit signal, and measuring the output against a particular choice of receive signal.

It is shown in [17] that if the two bodies are hyperrectangles with sides parallel to the x, y, z axes, there is a simple expression for Γ. More specifically, the eigenfunctions of the channel may be expressed in terms of a focusing function and a set of prolate spheroidal functions that are all easily computable. These eigenfunctions form a set of complete orthonormal functions in their respective volumes. Further, the corresponding eigenvalues have roughly a constant magnitude up to a critical number, after which the magnitudes are negligible. This critical number determines the number of communication modes between V_{T} and V_{R} and is given by

$$n_{\mathrm{c}} = \frac{V_{\mathrm{R}} V_{\mathrm{T}}}{D^2 \lambda^2 (2\Delta z_{\mathrm{T}})(2\Delta_{\mathrm{R}})} \tag{1}$$

where V_{T} and V_{R} are the volumes of the two bodies (with some abuse of notation), $2\Delta z_{\mathrm{T}}$ and $2\Delta z_{\mathrm{R}}$ are their thicknesses in the z direction, and λ is the signal wavelength. Consequently, the transfer function between V_{T} and V_{R} is given by a diagonal matrix of a finite dimension, with the diagonal elements being the nonnegligible eigenvalues.

A. Transfer Function

Let $\Psi(\mathbf{r}_{\mathrm{T}})$ be a transmit signal at any point $\mathbf{r}_{\mathrm{T}} \in V_{\mathrm{T}}$ and $\Phi(\mathbf{r}_{\mathrm{R}})$ be the electrical potential of the received signal at any point $\mathbf{r}_{\mathrm{R}} \in V_{\mathrm{R}}$. Then, we have

$$\Phi(\mathbf{r}_{\mathrm{R}}) = \int_{V_{\mathrm{T}}} G(\mathbf{r}_{\mathrm{R}}, \mathbf{r}_{\mathrm{T}}) \Psi(\mathbf{r}_{\mathrm{T}}) d^3\mathbf{r}_{\mathrm{T}} \tag{2}$$

where $G(\cdot,\cdot)$ is the retarded Green's function defined by

$$G(\mathbf{r}_{\mathrm{R}}, \mathbf{r}_{\mathrm{T}}) = \frac{\exp(-\iota k|\mathbf{r}_{\mathrm{R}} - \mathbf{r}_{\mathrm{T}}|)}{4\pi|\mathbf{r}_{\mathrm{R}} - \mathbf{r}_{\mathrm{T}}|} \tag{3}$$

where $\iota = \sqrt{-1}$ and $k = 2\pi/\lambda$, where λ is the wavelength of the signal. Let $\{\psi_{\mathrm{T}i}(\mathbf{r}_{\mathrm{T}}), i = 1, \ldots, N_{\mathrm{T}}\}$ (respectively, $\{\phi_{\mathrm{R}j}(\mathbf{r}_{\mathrm{R}}), j = 1, \ldots, N_{\mathrm{R}}\}$) be a finite set of orthonormal functions in V_{T} (respectively, V_{R}). Then, given any $\psi_{\mathrm{T}i}(\mathbf{r}_{\mathrm{T}})$, the received signal is given by

$$\Phi_{\mathrm{i}}(\mathbf{r}_{\mathrm{R}}) = \int_{V_{\mathrm{T}}} G(\mathbf{r}_{\mathrm{R}}, \mathbf{r}_{\mathrm{T}}) \psi_{\mathrm{T}i}(\mathbf{r}_{\mathrm{T}}) d^3\mathbf{r}_{\mathrm{T}}. \tag{4}$$

Define the projection of $\Phi_{\mathrm{i}}(\mathbf{r}_{\mathrm{R}})$ on $\phi_{\mathrm{R}j}(\mathbf{r}_{\mathrm{R}})$ as follows:

$$\Gamma_{ji} = \int_{V_{\mathrm{R}}} \int_{V_{\mathrm{T}}} \phi^*_{\mathrm{R}j}(\mathbf{r}_{\mathrm{R}}) G(\mathbf{r}_{\mathrm{R}}, \mathbf{r}_{\mathrm{T}}) \psi_{\mathrm{T}i}(\mathbf{r}_{\mathrm{T}}) d^3\mathbf{r}_{\mathrm{T}} d^3\mathbf{r}_{\mathrm{R}} \tag{5}$$

then, we have

$$\Phi_{\mathrm{i}}(\mathbf{r}_{\mathrm{R}}) = \sum_{j=1}^{N_{\mathrm{R}}} \Gamma_{ji} \phi_{\mathrm{R}j}(\mathbf{r}_{\mathrm{R}}) + \delta\Phi(\mathbf{r}_{\mathrm{R}}) \tag{6}$$

where $\delta\Phi(\mathbf{r}_{\mathrm{R}})$ is a residual term orthogonal to all $\phi_{\mathrm{R}j}(\mathbf{r}_{\mathrm{R}})$.We may write any transmit signal as

$$\Psi(\mathbf{r}_{\mathrm{T}}) = \sum_{i=1}^{N_{\mathrm{T}}} a_{\mathrm{i}} \psi_{\mathrm{T}i}(\mathbf{r}_{\mathrm{T}}). \tag{7}$$

The received signal is

$$\Phi(\mathbf{r}_{\mathrm{R}}) = \sum_{j=1}^{N_{\mathrm{R}}} b_j \phi_{\mathrm{R}j}(\mathbf{r}_{\mathrm{R}}) + \delta\Phi(\mathbf{r}_{\mathrm{R}}) \tag{8}$$

where $\delta\Phi(\mathbf{r}_{\mathrm{R}})$ is a residual signal orthogonal to all $\phi_{\mathrm{R}j}(\mathbf{r}_{\mathrm{R}})$ and

$$b_j = \sum_{i=1}^{N_{\mathrm{T}}} a_{\mathrm{i}} \Gamma_{ji}. \tag{9}$$

In a vector form, we have

$$\begin{bmatrix} b_1 \\ \vdots \\ b_{N_{\mathrm{R}}} \end{bmatrix} = \begin{bmatrix} \Gamma_{11} & \cdots & \Gamma_{1N_{\mathrm{T}}} \\ \vdots & \cdots & \vdots \\ \Gamma_{N_{\mathrm{R}}1} & \cdots & \Gamma_{N_{\mathrm{R}}N_{\mathrm{T}}} \end{bmatrix} \begin{bmatrix} a_1 \\ \vdots \\ a_{N_{\mathrm{T}}} \end{bmatrix} \tag{10}$$

or in a compact form

$$b = \Gamma a. \tag{11}$$

If the sets $\{\psi_{\mathrm{T}i}(\mathbf{r}_{\mathrm{T}}), i = 1, 2, \ldots\}$ and $\{\phi_{\mathrm{R}j}(\mathbf{r}_{\mathrm{R}}), j = 1, 2, \ldots\}$ are complete, then any transmit signal can be expressed as in (8) without the residual term $\delta\Phi(\mathbf{r}_{\mathrm{R}})$. In this case, (11) represents the true transfer function of the communication system, regardless of the choice of the basis functions $\{\psi_{\mathrm{T}i}(\mathbf{r}_{\mathrm{T}})\}$ and $\{\phi_{\mathrm{R}j}(\mathbf{r}_{\mathrm{R}})\}$.

Completeness of the function sets requires N_{T} and N_{R} to be infinite—and consequently, Γ is infinite dimensional. However, the channel between two finite volumes has a finite number of communication modes [17], [19]. Equivalently, the number of nonnegligible singular values of Γ is finite. If we choose the eigenfunctions of the channel $\{\varphi_{\mathrm{T}i}(\mathbf{r}_{\mathrm{T}})\}_{i=1}^{\infty}$ as our basis functions for the transmit signal, then the transfer matrix Γ is diagonal with σ_{i} as the entries, ordered from largest magnitude to smallest. Further, the number of communication modes n_c correspond to the number of nonnegligible singular values.

The functions $\varphi_{\mathrm{T}i}(\mathbf{r}_{\mathrm{T}})$ may be found through the analytic solution of an eigenvalue problem [17]

$$\sigma_{\mathrm{i}}^2 \varphi_{\mathrm{T}i}(\mathbf{r}'_{\mathrm{T}}) = \int\limits_{V_{\mathrm{T}}} \int\limits_{V_{\mathrm{R}}} G^*(\mathbf{r}_{\mathrm{R}}, \mathbf{r}_{T2}) G(\mathbf{r}_{\mathrm{R}}, \mathbf{r}_{T1}) \times \varphi_{\mathrm{T}i}(\mathbf{r}_{\mathrm{T}}) d^3\mathbf{r}_{\mathrm{R}} d^3\mathbf{r}_{\mathrm{T}} \tag{12}$$

where $\varphi_{\mathrm{T}i}(\mathbf{r}_{\mathrm{T}})$ is the ith (normalized) eigenfunction and the set $\{\varphi_{\mathrm{T}i}(\mathbf{r}_{\mathrm{T}})\}_{i=1}^{\infty}$ is a complete orthonormal set. However, this problem has tractable analytical solutions in only a small number of carefully designed geometric situations. The difficulty lies in computing these eigenfunctions when we have arbitrary bodies V_{T} and V_{R}.

Because the dimensions of the bodies are much smaller than the distance D, we use a paraxial approximation [17] to simplify $G(\mathbf{r}_{\mathrm{R}}, \mathbf{r}_{\mathrm{T}})$. We write the basis functions as [17]

$$\psi_{\mathrm{T}i}(\mathbf{r}_{\mathrm{T}}) = F_{\mathrm{T}}(\mathbf{r}_{\mathrm{T}}) \beta_{\mathrm{T}i}(\mathbf{r}_{\mathrm{T}}) \tag{13}$$

where $\beta_{\mathrm{T}i}(\cdot)$ are new functions and $F_{\mathrm{T}}(\cdot)$ is the so-called focusing function defined by

$$F_{\mathrm{T}}(\mathbf{r}_{\mathrm{T}}) = \exp\left(-\iota k \left(z_{\mathrm{T}} - \frac{x_{\mathrm{T}}^2}{2D} - \frac{y_{\mathrm{T}}^2}{2D}\right)\right) \tag{14}$$

so we may write (with some abuse of notation)

$$\beta_{\mathrm{T}i}(\mathbf{r}_{\mathrm{T}}) \equiv \beta_{\mathrm{T}i}(x_{\mathrm{T}}, y_{\mathrm{T}}) \tag{15}$$

and similarly for $\beta_{\mathrm{R}j}(x_{\mathrm{R}}, y_{\mathrm{R}})$. Each eigenfunction $\psi_{\mathrm{T}i}(\mathbf{r}_{\mathrm{T}})$—or $\phi_{\mathrm{R}j}(\mathbf{r}_{\mathrm{R}})$—is the product of a three-dimensional (3-D) focusing function and a two-dimensional (2-D) function. This is a crucial step towards numerical solutions for the transfer function between V_{T} and V_{R}.

We wish to find a computationally efficient method for determining the channel eigenfunctions. We note that while direct numerical solution (12) for arbitrary volumes is not efficient, we may use the analytic results of [17] to provide a significant computational saving in our numerical solution. To motivate our numerical solutions, we first consider the case where both V_{T} and V_{R} are hyperrectangles parallel to the x, y, z axes. Suppose the dimensions of V_{T} are given by $2\Delta x_{\mathrm{T}}$, $2\Delta y_{\mathrm{T}}$, and $2\Delta z_{\mathrm{T}}$, and similarly for V_{R}. This case is analyzed in [17] and the solution is given as

$$\beta_{\mathrm{T}i}(x_{\mathrm{T}}, y_{\mathrm{T}}) = \frac{S_{0m}(c_x, \hat{x}_{\mathrm{T}}) S_{0n}(c_y, \hat{y}_{\mathrm{T}})}{\sqrt{\Delta x_{\mathrm{T}} \Delta y_{\mathrm{T}} \Delta z_{\mathrm{T}}}} \tag{16}$$

for $m, n = 0, 1, \ldots$, where

$$c_x = \frac{k \Delta x_{\mathrm{T}} \Delta x_{\mathrm{R}}}{D} \tag{17}$$

and similarly for c_y and

$$\hat{x}_{\mathrm{T}} = \frac{x_{\mathrm{T}}}{\Delta x_{\mathrm{T}}} \tag{18}$$

and similarly for $\hat{y}_T$. The function $S_{0m}(c, \xi)$ is the so-called $(0, m)$th angular prolate spheroidal function [20], [21] with eigenvalues $v_m$that are well studied. The eigenvalues obey the relation

$$1 > |v_1| > |v_2| > \cdots > 0. \tag{19}$$

Only a finite number of v_{i} have nonnegligible magnitudes and for fixed values of c, the v_{i} fall off rapidly for $i > 2c/\pi$ [21]. Further, functions $\{S_{0m}(c, \xi)\}_{i=1}^{\infty}$ are complete and orthonormal over the unit interval. Computational methods for v_m and $S_{0m}(c, \xi)$ are available in [20] and [22].

B. Numerical Solutions for Arbitrary Volumes

Consider now the (general) case where V_{T} and V_{R} have arbitrary shapes, i.e., they are no longer prisms aligned along the z-axis. In this case, the basis functions $\beta_{\mathrm{T}i}(x_{\mathrm{T}}, y_{\mathrm{T}})$ (or $\beta_{\mathrm{R}i}(x_{\mathrm{R}}, y_{\mathrm{R}})$) cannot be separated (analytically) into x and y components of the form given by (16). We need to resort

to a numerical solution. We achieve this by modifying the eigenfunctions of the prism case to avoid solving (12) directly.

1) Project V_{T} along the z direction to obtain a surface S_{T} on the xy plane.
2) Define $\overline{S_{\mathrm{T}}}$ to be the smallest rectangle, with sides parallel to the xy axes, in the xy plane that covers S_{T}.
3) The side lengths $2\Delta x_{\mathrm{T}}$ and $2\Delta y_{\mathrm{T}}$ are the lengths of $\overline{S_{\mathrm{T}}}$ in the x and y directions, respectively.
4) The process is repeated for V_{R} to obtain S_{R}, $\overline{S_{\mathrm{R}}}$, $2\Delta x_{\mathrm{R}}$, and $2\Delta y_{\mathrm{R}}$.

We now have two rectangular surfaces that may be used to generate functions $\bar{\beta}_{\mathrm{T}i}(x_{\mathrm{T}}, y_{\mathrm{T}})$ and $\bar{\beta}_{\mathrm{R}i}(x_{\mathrm{R}}, y_{\mathrm{R}})$, substituting the "volumes" $\overline{V_{\mathrm{T}}} = \overline{S_{\mathrm{T}}} \times \max(2\Delta z_{\mathrm{T}})$ and $\overline{V_{\mathrm{R}}} = \overline{S_{\mathrm{R}}} \times \max(2\Delta z_{\mathrm{R}})$ in (16).

The "new" functions $\bar{\beta}_{\mathrm{T}i}(x_{\mathrm{T}}, y_{\mathrm{T}})$ and $\bar{\beta}_{\mathrm{R}i}(x_{\mathrm{R}}, y_{\mathrm{R}})$ are complete in both S_{T} and $\overline{S_{\mathrm{T}}}$, although not necessarily orthogonal or orthonormal. To see this, extend any function $f(x_{\mathrm{T}}, y_{\mathrm{T}})$, defined over S_{T}, to a function $g(x_{\mathrm{T}}, y_{\mathrm{T}})$, defined over the whole rectangle $\overline{S_{\mathrm{T}}}$ by

$$g(x_{\mathrm{T}}, y_{\mathrm{T}}) = \begin{cases} f(x_{\mathrm{T}}, y_{\mathrm{T}}), & (x_{\mathrm{T}}, y_{\mathrm{T}}) \in S_{\mathrm{T}} \subseteq \overline{S_{\mathrm{T}}} \\ 0, & \text{otherwise} \end{cases}. \quad (20)$$

Then, $g(x_{\mathrm{T}}, y_{\mathrm{T}})$ may be expressed as a linear combination of $\{\bar{\beta}_{\mathrm{T}i}(x_{\mathrm{T}}, y_{\mathrm{T}})\}$ over $\overline{S_{\mathrm{T}}}$, since $\{\bar{\beta}_{\mathrm{T}i}(x_{\mathrm{T}}, y_{\mathrm{T}})\}$ is a complete set in $\overline{S_{\mathrm{T}}}$, i.e., $g(x_{\mathrm{T}}, y_{\mathrm{T}}) = \sum_{\mathrm{i}} \alpha_{\mathrm{i}} \bar{\beta}_{\mathrm{T}i}(x_{\mathrm{T}}, y_{\mathrm{T}})$. The same combination $\{\alpha_1, \ldots\}$ still holds over S_{T} because $S_{\mathrm{T}} \subset \overline{S_{\mathrm{T}}}$. A similar claim holds for $\beta_{\mathrm{R}}(x_{\mathrm{R}}, y_{\mathrm{R}})$.

The set $\{\bar{\beta}_{\mathrm{T}i}(x_T, x_y)\}$ may be transformed to a complete and orthonormal set $\{\widetilde{\beta_{\mathrm{T}i}}(x_{\mathrm{T}}, y_{\mathrm{T}})\}$ in V_{T} using the Gram–Schmidt process. The norm is taken over V_{T}, i.e.,

$$\widetilde{\beta_{T1}}(x_{\mathrm{T}}, y_{\mathrm{T}}) = \frac{\bar{\beta}_{T1}(x_{\mathrm{T}}, y_{\mathrm{T}})}{\left\|\bar{\beta}_{T1}(x_{\mathrm{T}}, y_{\mathrm{T}})\right\|_{V_{\mathrm{T}}}} \quad (21)$$

where the volume integral in V_{T} may be simplified to a scaled surface integral on $\overline{S_{\mathrm{T}}}$

$$\begin{aligned} \|f(x_{\mathrm{T}}, y_{\mathrm{T}})\|_{V_{\mathrm{T}}}^2 &= \int_{V_{\mathrm{T}}} f^*(x_{\mathrm{T}}, y_{\mathrm{T}}) f(x_{\mathrm{T}}, y_{\mathrm{T}}) dx_{\mathrm{T}} dy_{\mathrm{T}} dz_{\mathrm{T}} \\ &\approx \int_{\overline{S_{\mathrm{T}}}} 2\Delta z_{\mathrm{T}}(x_{\mathrm{T}}, y_{\mathrm{T}}) f^*(x_{\mathrm{T}}, y_{\mathrm{T}}) \\ &\quad \cdot f(x_{\mathrm{T}}, y_{\mathrm{T}}) dx_{\mathrm{T}} dy_{\mathrm{T}} \end{aligned} \quad (22)$$

and $2\Delta z_{\mathrm{T}}(x_{\mathrm{T}}, y_{\mathrm{T}})$ is the "thickness" of V_{T} in the z direction at point $(x_{\mathrm{T}}, y_{\mathrm{T}})$. We transform the set $\{\bar{\beta}_{\mathrm{R}j}(x_{\mathrm{R}}, y_{\mathrm{R}})\}$ to a complete orthonormal set $\{\widetilde{\beta_{\mathrm{R}j}}(x_{\mathrm{R}}, y_{\mathrm{R}})\}$ in a similar way.

We now apply the paraxial approximation, which allows us to write the 3D basis functions in terms of the 2D functions $\beta_{\mathrm{T}}(x_{\mathrm{T}}, y_{\mathrm{T}})$ and a focusing function

$$\tilde{\psi}_{\mathrm{T}i}(\mathbf{r}_{\mathrm{T}}) = F_{\mathrm{T}}(\mathbf{r}_{\mathrm{T}}) \widetilde{\beta_{\mathrm{T}i}}(x_{\mathrm{T}}, y_{\mathrm{T}}) \quad (23)$$

and similarly

$$\tilde{\phi}_{\mathrm{R}j}(\mathbf{r}_{\mathrm{R}}) = F_{\mathrm{R}}(\mathbf{r}_{\mathrm{R}}) \widetilde{\beta_{\mathrm{R}j}}(x_{\mathrm{R}}, y_{\mathrm{R}}). \quad (24)$$

We approximate the Green's function in terms of the transmit and receive focusing functions [17]

$$G(\mathbf{r}_{\mathrm{R}}, \mathbf{r}_{\mathrm{T}}) \approx \frac{\mathrm{e}^{-\iota k D}}{4\pi D} F_{\mathrm{T}}^*(\mathbf{r}_{\mathrm{T}}) \mathrm{e}^{\frac{\iota k}{D}(x_{\mathrm{R}} x_{\mathrm{T}} + y_{\mathrm{R}} y_{\mathrm{T}})} F_{\mathrm{R}}(\mathbf{r}_{\mathrm{R}}). \quad (25)$$

It follows that

$$\begin{aligned} \Gamma_{ji} = \frac{\exp(-\iota k D)}{4\pi D} &\times \int_{V_{\mathrm{R}}} \int_{V_{\mathrm{T}}} \widetilde{\beta_{\mathrm{R}j}}^*(x_{\mathrm{R}}, y_{\mathrm{R}}) \exp\left(\frac{\iota k}{D}(x_{\mathrm{R}} x_{\mathrm{T}} + y_{\mathrm{R}} y_{\mathrm{T}})\right) \\ &\times \widetilde{\beta_{\mathrm{T}i}}(x_{\mathrm{T}}, y_{\mathrm{T}}) dx_{\mathrm{T}} dy_{\mathrm{T}} dz_{\mathrm{T}} dx_{\mathrm{R}} dy_{\mathrm{R}} dz_{\mathrm{R}}. \end{aligned} \quad (26)$$

Since the integrand is independent of z_{T} and z_{R}, we simplify

$$\begin{aligned} \Gamma_{ji} = \frac{\exp(-\iota k D)}{4\pi D} &\int_{S_{\mathrm{R}}} 2\Delta z_{\mathrm{R}}(x_{\mathrm{R}}, y_{\mathrm{R}}) \\ &\times \widetilde{\beta_{\mathrm{R}j}}^*(x_{\mathrm{R}}, y_{\mathrm{R}}) h(x_{\mathrm{R}}, y_{\mathrm{R}}) dx_{\mathrm{R}} dy_{\mathrm{R}} \end{aligned} \quad (27)$$

where

$$\begin{aligned} h(x_{\mathrm{R}}, y_{\mathrm{R}}) = &\int_{S_{\mathrm{T}}} 2\Delta z_{\mathrm{T}}(x_{\mathrm{T}}, y_{\mathrm{T}}) \exp\left(\frac{\iota k}{D}(x_{\mathrm{R}} x_{\mathrm{T}} + y_{\mathrm{R}} y_{\mathrm{T}})\right) \\ &\times \widetilde{\beta_{\mathrm{T}i}}(x_{\mathrm{T}}, y_{\mathrm{T}}) dx_{\mathrm{T}} dy_{\mathrm{T}}. \end{aligned} \quad (28)$$

In the above, $2\Delta z_{\mathrm{T}}(x_{\mathrm{T}}, y_{\mathrm{T}})$ is the thickness of V_{T} in the z direction at $(x_{\mathrm{T}}, y_{\mathrm{T}})$, and $2\Delta z_{\mathrm{R}}(x_{\mathrm{R}}, y_{\mathrm{R}})$ is similarly defined. The benefit of decomposing the integral as shown is that we may significantly reduce the computation required to compute Γ_{ji} since we may compute $h(x_{\mathrm{R}}, y_{\mathrm{R}})$ using (28) once, for each basis function in V_{T}. This function is then constant in (27) for each basis function in V_{R}.

The functions $\widetilde{\beta_{\mathrm{T}i}}(x_{\mathrm{T}}, y_{\mathrm{T}})$ and $\widetilde{\beta_{\mathrm{R}j}}(x_{\mathrm{T}}, y_{\mathrm{T}})$ are not eigenfunctions of the channel between V_{T} and V_{R}, rather they are eigenfunctions of the channel between $\overline{V_{\mathrm{T}}}$ and $\overline{V_{\mathrm{R}}}$. Consequently, the transfer matrix Γ is not diagonal. However, when S_{T} and S_{R} are close to their bounding sets $\overline{S_{\mathrm{T}}}$ and $\overline{S_{\mathrm{R}}}$, respectively, and the thicknesses $\Delta z_{\mathrm{T}}(x_{\mathrm{T}}, y_{\mathrm{T}})$ and $\Delta z_{\mathrm{R}}(x_{\mathrm{R}}, y_{\mathrm{R}})$ are roughly constant, the eigenfunctions corresponding to $(V_{\mathrm{T}}, V_{\mathrm{R}})$ are similar to those corresponding to $(\overline{V_{\mathrm{T}}}, \overline{V_{\mathrm{R}}})$. As such, we may manipulate Γ through the singular-value decomposition (SVD) to obtain the correct basis functions.

C. Simplification of Transfer Function

In practice, only a finite number of terms of Γ_{ji} are computed, i.e., we obtain a truncated Γ. In order to measure the accuracy of Γ, we resort to the sum rule of [17].

Suppose $\{\tilde{\psi}_{\mathrm{T}i}(\mathbf{r}_{\mathrm{T}}), i = 1, 2, \ldots\}$ and $\{\tilde{\phi}_{\mathrm{R}j}(\mathbf{r}_{\mathrm{R}}), i = 1, 2, \ldots\}$ are any two sets of orthonormal functions for V_{T} and V_{R}, respectively, then (by Parseval's theorem) for free-space transmission

$$\sum_{i,j} |\Gamma_{ji}|^2 \leq \frac{1}{(4\pi)^2} \int_{V_{\mathrm{T}}} \int_{V_{\mathrm{R}}} \frac{1}{|\mathbf{r}_{\mathrm{R}} - \mathbf{r}_{\mathrm{T}}|^2} d^3\mathbf{r}_{\mathrm{T}} d^3\mathbf{r}_{\mathrm{R}} \quad (29)$$

with equality if and only if the sets are complete. Under the assumption that the dimensions of V_{T} and V_{R} are sufficiently small compared to the separating distance D, (29) becomes

$$\sum_{i,j} |\Gamma_{ji}|^2 \leq \frac{V_{\mathrm{T}} V_{\mathrm{R}}}{(4\pi D)^2} \tag{30}$$

$$= \sum_{\mathrm{i}}^{N} \sum_{j}^{N} |\Gamma_{ji}|^2 + \delta_E, \qquad \delta_E > 0. \tag{31}$$

From (31), if δ_E is sufficiently[1] small, then the finite estimation of Γ is sufficiently accurate. If δ_E is too large (the sum of $|\Gamma_{ji}|^2$ is too small), then we increase the number of basis functions and compute a larger dimension Γ. By the orthogonality of the basis functions, we may simply append the additional terms onto the matrix Γ. As a rule of thumb, we choose the dimension of the truncated Γ to be $\bar{n_{\mathrm{c}}} \times \bar{n_{\mathrm{c}}}$, where $\bar{n_{\mathrm{c}}}$ is the number of communication modes for $(\overline{S_{\mathrm{T}}}, \overline{S_{\mathrm{R}}})$. Recall from (1)

$$\bar{n_{\mathrm{c}}} = \frac{\overline{S_{\mathrm{R}}} \cdot \overline{S_{\mathrm{T}}}}{D^2 \lambda^2}. \tag{32}$$

We then increase the dimension of Γ, if necessary, according to (31).

In general, the dimension of Γ as obtained above is larger than the number of communication modes for $(V_{\mathrm{T}}, V_{\mathrm{R}})$. This is because $\tilde{\psi}_{\mathrm{T}i}(\mathbf{r}_{\mathrm{T}})$ and $\tilde{\phi}_{\mathrm{R}j}(\mathbf{r}_{\mathrm{R}})$ are not necessarily the eigenfunctions for $(V_{\mathrm{T}}, V_{\mathrm{R}})$. In order to obtain a minimal representation of Γ, we perform a singular-value decomposition, i.e., we form

$$\Gamma = U^* \Lambda V \tag{33}$$

where U and V are unitary matrices and Λ is a diagonal matrix containing the singular values of Γ in descending-magnitude order. We may generate the optimal-diagonalizing-basis sets by application of V and U

$$\psi_{\mathrm{T}i}^{\mathrm{opt}}(\mathbf{r}_{\mathrm{T}}) = \sum_{j} \tilde{\psi}_{Tj}(\mathbf{r}_{\mathrm{T}}) V_{i,j} \tag{34}$$

$$\phi_{\mathrm{R}i}^{\mathrm{opt}}(\mathbf{r}_{\mathrm{R}}) = \sum_{j} \tilde{\phi}_{\mathrm{R}j}(\mathbf{r}_{\mathrm{R}}) U_{i,j} \tag{35}$$

which means that the basis functions are now the eigenfunctions of the channel. After the decomposition (33), we may have several negligible singular values. These may be discarded to provide a reduced-transfer function. The number of remaining terms corresponds to the number of communication modes for the system.

The unitary matrices U and V may be interpreted as optimal energy distributions for the (suboptimal) basis functions used, i.e., if we were forced to transmit using signals $\tilde{\psi}_{\mathrm{T}}(\mathbf{r}_{\mathrm{T}})$ and forced to receive using $\tilde{\psi}_{\mathrm{T}}(\mathbf{r}_{\mathrm{T}})$, then U and V would provide "steering" for our signals to ensure that the appropriate channel modes were activated.

[1]For simulations, we chose $\delta_E < 1 \times 10^{-8}$ as a threshold.

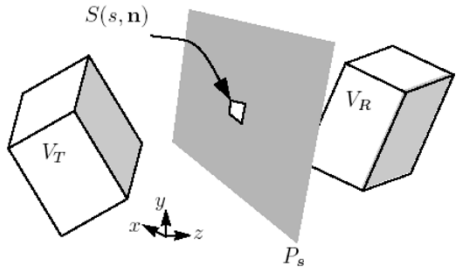

Fig. 2. Two-volume arrangement, with absorbing plane P_s and finite hole $S(s,\mathbf{n})$. Size of $S(s,\mathbf{n})$ determines scatterer size.

III. Modeling for Volume Communications With Scattering Bodies

A. An Imaginary Exercise

Consider the two volume communication system in Fig. 2, where we have placed an infinitely large absorbing plane P_s at point s between V_{T} and V_{R}. The normal direction $\mathbf{n}$ of P_s is arbitrary. The plane is fully energy absorbing except for a hole $S(s,\mathbf{n})$ in the middle, i.e., the only means for any signal to reach V_{R} from V_{T} is through $S(s,\mathbf{n})$. We ask "how large must this hole be so that communication between the two volumes is not affected?"

The answer to this question is as follows: If λ is sufficiently small, then $S(s,\mathbf{n})$ is the minimum area containing all the intersection points of P_s and $\ell(\mathbf{r}_{\mathrm{T}}, \mathbf{r}_{\mathrm{R}})$, where $\ell(\mathbf{r}_{\mathrm{T}}, \mathbf{r}_{\mathrm{R}})$ is a line linking $\mathbf{r}_{\mathrm{T}} \in V_{\mathrm{T}}$ and $\mathbf{r}_{\mathrm{R}} \in V_{\mathrm{R}}$. If λ is not small compared with $S(s,\mathbf{n})$, then $S(s,\mathbf{n})$ must be enlarged by several wavelengths so that fringing and diffractions on the edges are negligible. We denote $S(s,\mathbf{n})$ as the viewing area (with respect to P_s). If we replace the finite "hole" with a "scatterer," we have the smallest size scatterer, allowing all possible communication modes between V_{T} and V_{R}. Smaller scatterers will only allow partial communication.

B. Single Scatterer

Now we consider the scenario where there is a single scatterer S, as depicted in Fig. 3. We assume that S is a (purely) reflective plane, i.e., there is no penetration of the electromagnetic field, using a similar model to that of [23]. This simplification ignores the specular effects of scattering through clouds of small particles. However, modeling scatterers as pure reflectors becomes exact as the total path length, via a single scatterer, becomes large with respect to the signal wavelength [24].

The reflective nature of S means that the reflection angle θ_{r} is the same as the incident angle θ_{i}. The reflection involves a loss that is represented by the following gain, cf. [25]

$$\eta(\theta_{\mathrm{i}}) = \exp\left\{ \left(\frac{\pi}{\lambda} \sigma_h \cos\theta_{\mathrm{i}} \right)^2 \right\} J_0\left\{ 8 \left(\frac{\pi}{\lambda} \sigma_h \cos\theta_{\mathrm{i}} \right)^2 \right\} \tag{36}$$

where σ_h is the standard deviation of the surface height, and $J_0(\cdot)$ is the modified Bessel function of order zero. Note that for a perfectly flat plane, $\sigma_h = 0$ and $\eta(\theta_{\mathrm{i}}) = 1$. The normal angle $\mathbf{n}$ of the scatterer must be such that the reflected signals

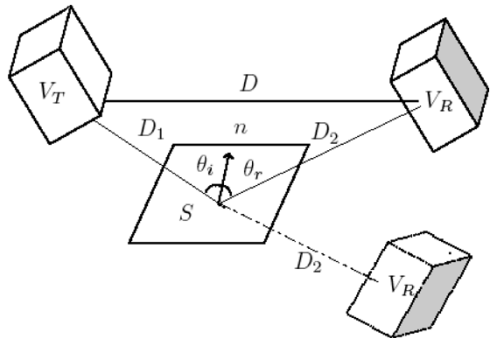

Fig. 3. Two-volume arrangement, with single finite reflective scatterer S.

are directed at V_{R}, so that signal transmission from V_{T} to V_{R} is possible.

To determine the field within V_{R}, we mirror-image the body V_{R} with respect to the scatterer to generate a virtual body V'_{R} (see Fig. 3). The scatterer S may be viewed as the "hole" through which communications between V_{T} and V'_{R} occurs. The area of S must be larger than the corresponding viewing area between V_{T} and V'_{R}, in order for V_{T} to fully communicate with V_{R}. Once this condition holds, the transfer function between V_{T} and V_{R} can be computed using the result in Section II-B. The algorithm becomes as follows.

Algorithm 1: Scatter channel model

1) The effective propagation distance is the total path length $D_s = D_1 + D_2$.
2) The mirror-image body V'_{R}—the rotated mirror-imaged copy of V_{R}—is substituted for V_{R}.
3) Using the propagation distance D_s and the receive body V'_{R}, the process of Section II-B is applied.
4) The computed eigenfunctions for V'_{R} are rotated and mirror-imaged back so that they become functions for V_{R}.

Note that the same result can be obtained by mirror-imaging V_{T}—to generate V'_{T}—due to the symmetry between transmit and receive volumes. Let us summarize the assumptions we use for the scatterer.

A1) The normal direction $\mathbf{n}$ of S is such that the reflected signals from V_{T} reach V_{R}.
A2) Each scatterer S is a (small) finite-size purely reflective plane with loss given by (36).
A3) The distance D_1 from V_{T} to S is sufficiently large compared to the size of S that for any point in V_{T}, the incident angle across the whole of S is roughly constant. A similar condition holds for D_2.
A4) Each scatterer is "local" to either V_{T} or V_{R}, i.e., either $D_1 \ll D$ or $D_2 \ll D$.

We note that it is possible to relax these assumptions, at the expense of increasing the model complexity. We make the following observations.

Obs1) A scatterer that is not appropriately aligned is equivalent to a smaller (appropriately aligned) scattering object.
Obs2) A scatterer S that is smaller than the necessary viewing area[2] reduces the communication strength for the path from V_{T} to V_{R} via S. Modeling is possible by considering only the "visible" part of V_{R}, i.e., by considering transmission between V_{T} and a smaller V_{R}. From (29), the reduction in effective volume reduces the number of communication modes for the link via this path.
Obs3) A scatterer S that is "too close"' that A3 does not hold may be considered as a collection of several smaller scattering bodies $\{S_1, S_2, \ldots\}$ such that A3 holds for each.
Obs4) Any scatterer S that is not local to either volume is ineffective for transmission.

To see Obs4 intuitively, when S is distant from both V_{T} and V_{R}, the added propagation distance makes the received signal significantly weaker. Further, the number of communications modes available (1) through a link via S is very small, due to the large propagation length independent of transmission power. Consequently, the link via S appears as a low-power link with a few degrees of freedom. This implies that a distant scatterer will not contribute new orthogonal modes. Although such a scatterer may improve the signal power received, the contribution is dominated by any local scattering.

The consequence of Obs4 is that we only need to consider scatterers that are local to V_{T} and/or V_{R}. A simple example of this approach is the well known ring-scatter model [26], [27]. An NLOS path (via a scatterer) may be comparable to the line-of-sight (LOS) path, provided that assumptions A1–A4 are satisfied and the reflection loss (36) is not significant.

C. Multiple Scatterers per Path

The model described above may be easily extended to the case where multiple reflections occur along a single path from V_{T} to V_{R}. For a given scatterer S, we may consider a virtual free-space transmission path P_S from V_{T} to V_{R}. The communication modes are given by Algorithm 1.

For a path containing more than one scatterer, we simply repeat the mirror imaging of V_{R} for each scattering body along the path. In this way, a virtual path is generated that incorporates the effect of each scattering body—concatenating the reflections and losses from each body—along the way. Having "unwound" the scattering path—performing a reflection for each scatterer and incrementing the virtual path length—the communication modes are calculated using Algorithm 1.

D. Multiple Paths

Consider the scenario in Fig. 4 with scatterers $S^{(k)}, k = 1, \ldots, K$, in accordance with assumptions A1–A4. Each scatterer provides a communication path and the transfer function $\Gamma^{(k)}$ for each path can be computed using the method in Section III-B. The true value of Γ cannot be obtained by directly summing the various $\Gamma^{(k)}$ transfer functions, because each $\Gamma^{(k)}$ uses different eigenfunctions.

[2]Either due to misalignment or small physical size.

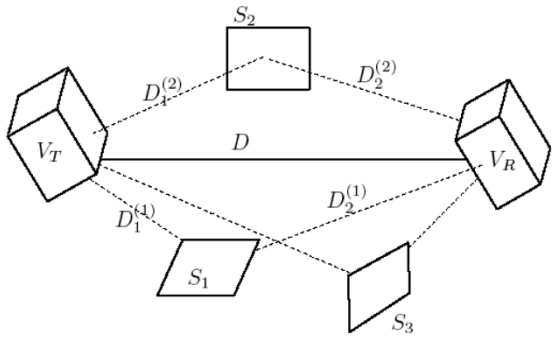

Fig. 4. Two-volume transmission, in the presence of multiple scatterers.

To obtain a correct Γ, we denote by $\{\psi_{\mathrm{T}i}^{(k)}(\mathbf{r}_{\mathrm{T}}), i = 1, 2, \ldots\}$ and $\{\phi_{\mathrm{R}j}^{(k)}(\mathbf{r}_{\mathrm{R}}), j = 1, 2, \ldots\}$ the two sets of eigenfunctions corresponding to $\Gamma^{(k)}$ and let the dimension of $\Gamma^{(k)}$ be $N_{\mathrm{c}}^{(k)} \times N_{\mathrm{c}}^{(k)}$. Then, we have the following mapping:

$$\left\{\psi_{\mathrm{T}i}^{(k)}(\mathbf{r}_{\mathrm{T}})\right\} \overset{\Gamma^{(k)}}{\longmapsto} \left\{\phi_{\mathrm{R}j}^{(k)}(\mathbf{r}_{\mathrm{R}})\right\}. \tag{37}$$

Let $\{\psi_{\mathrm{T}i}(\mathbf{r}_{\mathrm{T}})\}$ and $\{\phi_{\mathrm{R}j}(\mathbf{r}_{\mathrm{R}})\}$ be any sets of complete orthonormal basis functions for V_{T} and V_{R}, respectively. In particular, they may be the basis functions corresponding to the direct transmission path. We can project each $\psi_{\mathrm{T}i}^{(k)}(\mathbf{r}_{\mathrm{T}})$ onto $\psi_{Tj}(\mathbf{r}_{\mathrm{T}}), j = i, 2\cdots$ to obtain the following:

$$\psi_{\mathrm{T}i}^{(k)}(\mathbf{r}_{\mathrm{T}}) = \sum_{j=1}^{\infty} \Gamma_{ij}^{(k)} \psi_{\mathrm{T}j}(\mathbf{r}_{\mathrm{T}}) \tag{38}$$

where $\Gamma_{ij}^{(k)}$ are projection coefficients. In order to perform the projection, we first note that both the eigenfunctions $\psi_{\mathrm{T}i}^{(k)}(\mathbf{r}_{\mathrm{T}})$ and the focusing function of the rotated-mirror-imaged volumes must be projected back to a common reference.

Denote $F(x, y, z)$ as the original focusing function and $F^{(k)}(x, y, z)$ as the focusing function for path k—where we have already carried out the rotation and mirror-imaging—we may write

$$\Gamma_{ij}^{(k)} = \int_{V_{\mathrm{T}}} \psi_{\mathrm{R}i}^{(k)}(x_{\mathrm{T}}, y_{\mathrm{T}}) F^{(k)}(x, y, 0) F^{-1}(x, y, 0) \cdot \psi_{\mathrm{R}j}(x_{\mathrm{T}}, y_{\mathrm{T}}) dx\, dy\, dz. \tag{39}$$

In vector form, we have

$$\psi_{\mathrm{T}i}^{(k)}(\mathbf{r}_{\mathrm{T}}) = \Gamma_{\psi}^{(k)} \psi_{\mathrm{T}i}(\mathbf{r}_{\mathrm{T}}) \tag{40}$$

for some matrix $\Gamma_{\psi}^{(k)}$ with $N_{\mathrm{c}}^{(k)}$ columns and infinitely many rows. For numerical calculations, $\Gamma_{\psi}^{(k)}$ is truncated in similar form as Γ. Similarly, each function $\phi_{\mathrm{R}j}(\mathbf{r}_{\mathrm{R}})$ may be projected onto $\phi_{\mathrm{R}j}^{(k)}(\mathbf{r}_{\mathrm{R}}), j = 1, 2, \ldots$ to obtain

$$\phi_{\mathrm{R}j}(\mathbf{r}_{\mathrm{R}}) = \Gamma_{\phi}^{(k)} \phi_{\mathrm{R}j}^{(k)}(\mathbf{r}_{\mathrm{R}}) + \delta\phi_{\mathrm{R}}^{(k)}(\mathbf{r}_{\mathrm{R}}) \tag{41}$$

for some matrix $\Gamma_{\phi}^{(k)}$ with $N_{\mathrm{c}}^{(k)}$ rows and infinitely many columns, where $\delta\phi_{\mathrm{R}}^{(k)}(\mathbf{r}_{\mathrm{R}})$ is the residual term orthogonal to all $\phi_{\mathrm{R}j}^{(k)}(\mathbf{r}_{\mathrm{R}})$. The elements of $\Gamma_{\psi}^{(k)}$ and $\Gamma_{\phi}^{(k)}$ may be computed numerically.

With the above projections, we can express the mappings from $\psi_{\mathrm{T}}(\mathbf{r}_{\mathrm{T}})$to $\phi_{\mathrm{R}}(\mathbf{r}_{\mathrm{R}})$ through $S^{(k)}$ as follows:

$$\psi_{\mathrm{T}}(\mathbf{r}_{\mathrm{T}}) \overset{\Gamma_{\psi}^{(k)}}{\longmapsto} \psi_{\mathrm{T}}^{(k)}(\mathbf{r}_{\mathrm{T}}) \overset{\Gamma^{(k)}}{\longmapsto} \phi_{\mathrm{R}}^{(k)}(\mathbf{r}_{\mathrm{R}}) \overset{\Gamma_{\phi}^{(k)}}{\longmapsto} \phi_{\mathrm{R}}(\mathbf{r}_{\mathrm{R}}). \tag{42}$$

Thus, the overall transfer function is given by

$$\Gamma = \sum_{k=1}^{K} \Gamma_{\phi}^{(k)} \Gamma^{(k)} \Gamma_{\psi}^{(k)}. \tag{43}$$

The only difficulty is that there is no sum rule to determine the numerical accuracy of the computation, i.e., (29) is invalid for transmission in scattering environments. This implies that $\Gamma_{\phi}^{(k)}$ and $\Gamma_{\psi}^{(k)}$ must have large dimension to ensure numerical accuracy. Once Γ is obtained, the singular-value decomposition in (33) can be performed to obtain the eigenfunctions, singular values, and number of communication modes.

We may easily include an LOS path. Denote its transfer function and the corresponding projection matrices by $\Gamma^{(0)}$, $\Gamma_{\phi}^{(0)}$, and $\Gamma_{\psi}^{(0)}$, respectively. Then, (43) is modified to

$$\Gamma = \sum_{k=0}^{K} \Gamma_{\phi}^{(k)} \Gamma^{(k)} \Gamma_{\psi}^{(k)}. \tag{44}$$

Using (44), the direct transmission path is simply one of many possible transmission paths, each with their respective transfer-matrix and basis functions.

IV. Simulation

We compare a direct (nonscattering) transmission with various scattering environments. We consider a 3-GHz transmission frequency giving $\lambda = 0.1$ m. The volumes V_{T} and V_{R} are hyperrectangles. V_{T} has side lengths of $15\lambda \times 9\lambda \times 9\lambda$ and V_{R} has side lengths of $18\lambda \times 9\lambda \times 9\lambda$. The volumes are separated by $D = 10$ m. For this arrangement, the number of communications modes for direct transmission (1) is $N_{\mathrm{c}} \approx 2.6$. We have used [28] for the numerical computation of (16).

The arrangement has been deliberately chosen to ensure a small nonnegligible number of direct transmission modes to emphasize the effect of scattering. Physically, such a model may correspond to placing antenna elements within two office filing cabinets, and placing the cabinets within adjacent offices. Under this arrangement, we may ask "how many well-connected parallel channels exist between the filing cabinets?" Examining this question provides insight into the effect of scattering upon the wireless channel. The physical channel is of less importance than the concept of the continuous modes.

Fig. 5 shows the squared singular values for the different scattering environments. The squared singular values provide the channel gains for the effective parallel channels from V_{T}

to V_{R}. The singular values are not normalized, which allows comparison among the various channel scenarios.

The direct-transmission case is shown by the solid line. The singular values $\hat{\sigma}_k$ drop sharply beyond $k = 3$. This corresponds to the value of N_{c} for this arrangement. The first singular value $\sigma_1 = 0.0067$ represents the channel gain, and gives an indication of distance (and other) losses.

Using the same physical arrangement, we introduced scattering, in both an NLOS and LOS case. Scatterers were modeled as reflective planes with a gain (36), $\eta = 1$. Each scatterer was placed in a random location, between V_{T} and V_{R}, with a random orientation. Monte Carlo simulations were then used, to generate average-case results.

The NLOS transmission is shown by the solid line with squares. In this situation, transmission was possible only via the reflective scatterers, where $K = 20$ scatterers were used. Physically, this corresponds to using an absorbing region between V_{T} and V_{R} that prevents any direct transmission. It can be seen that the channel gain $\sigma_1 = 0.0058$ is similar to the direct-transmission case. As additional scatterers are introduced, this gain tends to increase—as the total signal power received at V_{R} increases with each additional path. Comparing the NLOS case with the direct-transmission case, scattering has provided approximately double the number of equal-strength communications modes. This can be seen by comparing the value k for which the direct-case singular values σ_{direct} and σ_{NLOS} fall below some threshold (say 1×10^{-3}). This corresponds to a significant improvement in the number of parallel channels. Equally, the relative magnitude of the singular values in the NLOS case is much smaller, which may be interpreted as a less correlated channel than the direct-transmission case.

This case may be compared with the single-scatterer NLOS channel, where a scatterer was placed randomly at a distance from both V_{T} and V_{R}. As can be seen, the channel gain in this case is significantly reduced. The pinhole channel suffers from two reductions in singular values.

1) The scatterer is at an angle to the volumes, so the number of well-connected modes is reduced (although there may be several poorly connected modes).
2) The distance from V_{T} to V_{R} is larger than the direct-transmission path length, so the gain is also reduced.

The LOS case is shown by the circled line. Here, communication occurred via both dense scattering ($K = 20$) and direct transmission. The channel gain $\sigma_1 = 0.0068$, and this can be seen in the same way as the channel-gain improvement in the NLOS case. Each scatterer provides an additional communication path, and consequently, additional signal power at the receiver. This is precisely the effect seen when using a parabolic-dish antenna around a radio transmitter: the presence of the dish improves the power gain of the point-to-point channel. Comparing with NLOS, we see a significant improvement in the number and strengths of effective communication modes as expected.

In Fig. 6, we have plotted the (normalized) magnitude of the first and second communication modes for a direct-transmission case Γ_{d}, pinhole NLOS case, Γ_{n} and LOS case, and Γ_{l} between the hyperrectangles V_{T} and V_{R} described in Section IV. The pinhole NLOS case was generated by placing a single scatterer along the diagonal of V_{T}, and the LOS case generated by combining both the direct and pinhole NLOS channels. It was assumed that the gain of the scatterer (36), was $\eta = 0.5$. The LOS channel and the direct channel are related by

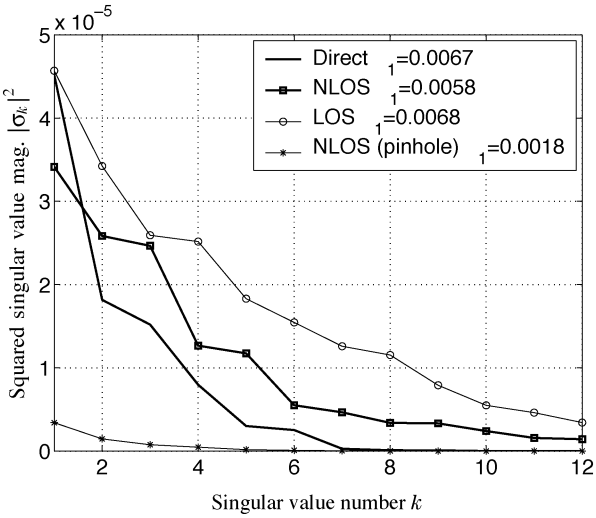

Fig. 5. Squared magnitudes of singular values of transfer operator Γ ranked in order of magnitude. Cases considered are direct (no scattering), NLOS (ten scatterers, transmission only via scattering bodies), LOS (ten scatterers plus direct transmission) and NLOS-pinhole (all transmission via single scatterer).

$$\Gamma_{\mathrm{l}} = \Gamma_{\mathrm{d}} + \frac{1}{2}\Gamma_{\psi}\Gamma_{\mathrm{n}}\Gamma_{\phi}. \tag{45}$$

We note that the low-order modes of the LOS scenario are similar to those of the direct (nonscattering) scenario, while the NLOS modes are significantly different.

V. Discussion

Let us consider two volumes in free space, i.e., the direct-transmission case. We have a set of basis functions, which may be calculated as described in Section II. Although there are infinitely many orthonormal functions in the sets $\psi_{\mathrm{T}i}(\mathbf{r}_{\mathrm{T}})$ and $\phi_{\mathrm{R}j}(\mathbf{r}_{\mathrm{R}})$, only a finite number n_{c} have nonnegligible connection strengths, corresponding to the well-connected modes.

For every scatterer $S^{(k)}$, a new pair of basis sets $\psi_{\mathrm{T}i}^{(k)}(\mathbf{r}_{\mathrm{T}})$ and $\phi_{\mathrm{R}j}^{(k)}(\mathbf{r}_{\mathrm{R}})$ are generated. These are not necessarily the same as those of the direct path. Some of the basis functions $\psi_{\mathrm{T}i}^{(k)}(\mathbf{r}_{\mathrm{T}})$ (and $\phi_{\mathrm{R}j}^{(k)}(\mathbf{r}_{\mathrm{R}})$) have components that are parallel to the well-connected direct-path modes and some have components that are orthogonal to all of the well-connected direct-path modes. Further, if the path length via $S^{(k)}$ is approximately equal to the direct-path length D, and the sizes of V_{T} and V_{R} are unchanged, each scatterer path has the same sum of path gains as the direct case (ignoring reflection loss) given by the sum rule.

The components of $\psi_{\mathrm{T}i}^{(k)}(\mathbf{r}_{\mathrm{T}})$ and $\phi_{\mathrm{R}j}^{(k)}(\mathbf{r}_{\mathrm{R}})$ that are orthogonal to existing eigenfunctions produce additional (orthogonal) modes of communication. These orthogonal modes correspond to additional parallel-communication channels that are unavailable for direct transmission. The remaining components (parallel to existing eigenfunctions) contribute to the gain of

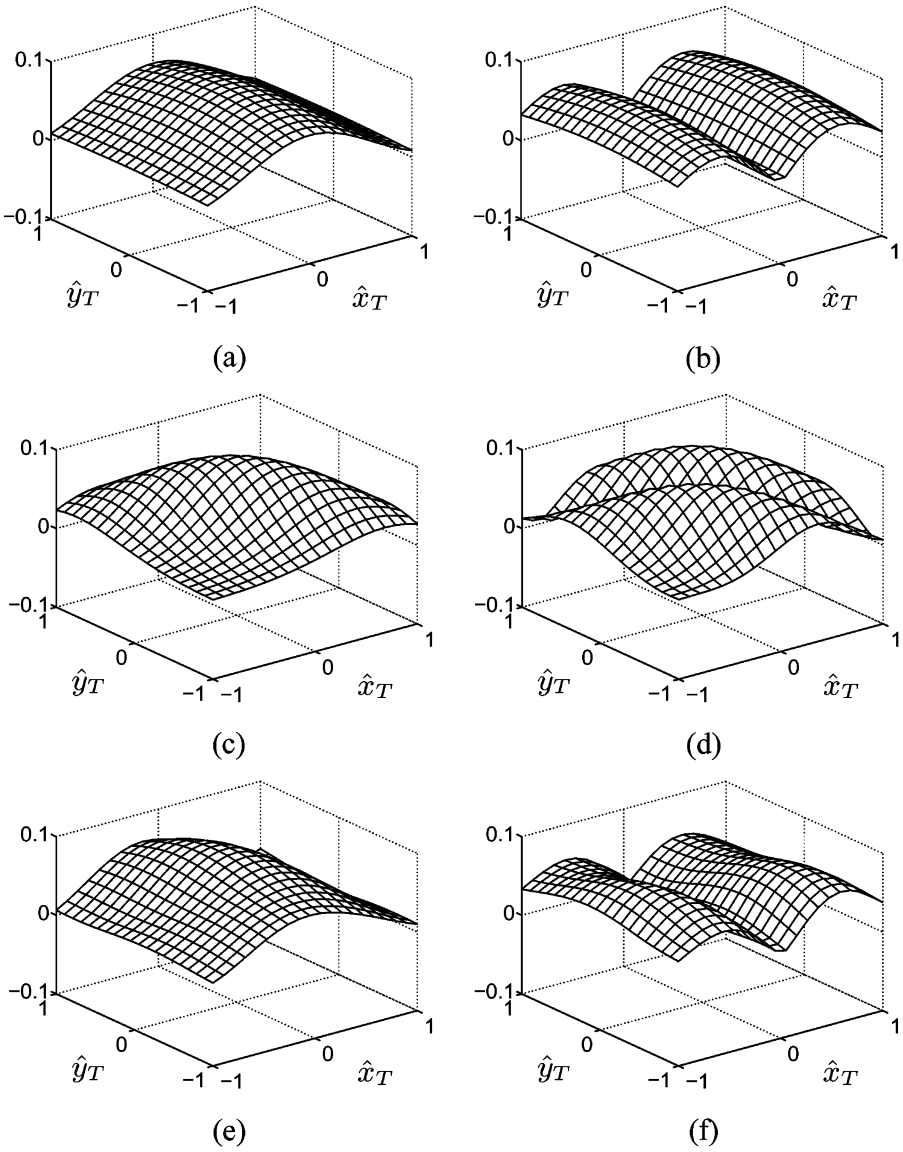

Fig. 6. Magnitude of low-order eigenmodes in V_{T} for direct transmission Γ_{d}, NLOS transmission Γ_{n}, and LOS Γ_{l} transmission. NLOS transmission via single scatterer. LOS matrix calculated according to $\Gamma_{\mathrm{l}} = \Gamma_{\mathrm{d}} + (1/2)\Gamma_{\psi}\Gamma_{\mathrm{n}}\Gamma_{\phi}$. Note similarity between direct modes and LOS modes. (a) Direct mode 1, $|\psi_{T1}^{(d)}(\mathbf{r}_{\mathrm{T}})|$. (b) Direct mode 2, $|\psi_{T2}^{(d)}(\mathbf{r}_{\mathrm{T}})|$. (c) NLOS mode 1, $|\psi_{T1}^{(n)}(\mathbf{r}_{\mathrm{T}})|$. (d) NLOS mode 2, $|\psi_{T2}^{(n)}(\mathbf{r}_{\mathrm{T}})|$. (e) LOS mode 1, $|\psi_{T1}^{(l)}(\mathbf{r}_{\mathrm{T}})|$. (f) LOS mode 2, $|\psi_{T2}^{(l)}(\mathbf{r}_{\mathrm{T}})|$.

the corresponding modes. The gain contribution may be either constructive or destructive, depending on phases. A particular example of this is the parabolic dish: the various pieces of the dish may be considered as reflective scatterers. No new modes of communication are created. However, the power gain of the channel is markedly improved over a free-space LOS case.

It is clear that we cannot increase the number of communication modes indefinitely because there is a finite area that can be illuminated by scattering—each scatterer shadows those behind it. The theoretical limit is reached when scatterers essentially act as a lens. As such, scattering provides improvements in channel capacity by:

1) increasing the gain of particular communication modes by constructive interference; and
2) increasing the number of well-connected communication modes.

VI. Conclusion

We have presented a numerical approach for the computation of the number and strength of communication modes between two arbitrary volumes. We have extended these numerical computations to account for transmission in the presence of reflective-scattering bodies. We have shown that multipath scattering may be modeled by iteratively considering each scatterer as a particular instance in a general multipath field. This has been used to provide an insight into the physical channel characteristics necessary to achieve "rich" scattering. We have shown that the continuous channel may be considered as the limiting case for densely placed receiver and transmitter elements.

We have shown that reflective scattering can improve channel capacity through a combination of two methods: increasing channel gains, and increasing the number of communication modes. The first case is predominant in the "pinhole" channel,

where scatterers are placed closely together. In this case, the number of communication modes are dominated by the direct transmission. In the second case, so-called "dense" scattering, where scatterers are placed randomly, provides additional orthogonal communication modes over those already present in direct transmission. Simulation results have been used to show the improvement scatterers provide to the low-order singular values of the transfer matrix, and the conditions under which scattering can increase the number of communication modes.

ACKNOWLEDGMENT

The authors would like to thank Nanyang Technological University for their support of this research.

REFERENCES

[1] G. J. Foschini and M. J. Gans, "On limits of wireless communications in a fading environment when using multiple antennas," *Wireless Pers. Commun.*, vol. 6, no. 3, pp. 311–335, Mar. 1998.

[2] I. E. Telatar, "Capacity of multi-antenna Gaussian channels," *Eur. Trans. Telecommun.*, vol. 10, no. 6, pp. 585–595, Nov. 1999.

[3] P. Wolniansky, G. Golden, G. J. Foschini, and R. Valenzuela, "V-BLAST: An architecture for realizing very high data rates over the rich-scattering wireless channel," in *URSI Int. Symp. Signals, Systems, Electronics (ISSSE)*, Pisa, Italy, Sep. 29–Oct. 2, 1998, pp. 295–300.

[4] H. Bölcskei, D. Gesbert, and A. Paulraj, "On the capacity of OFDM-based spatial multiplexing systems," *IEEE Trans. Commun.*, vol. 50, no. 2, pp. 225–234, Feb. 2002.

[5] D. Gesbert, H. Bölcskei, D. Gore, and A. Paulraj, "Outdoor MIMO wireless channels: Models and performance prediction," *IEEE Trans. Commun.*, vol. 50, no. 12, pp. 1926–1934, Dec. 2002.

[6] T. D. Abhayapala, R. A. Kennedy, and J. T. Y. Ho, "On capacity of multi-antenna wireless channels: Effects of antenna separation and spatial correlation," in *3rd Australian Communications Theory Workshop (AusCTW)*, Canberra, Australia, Feb. 4–5, 2002, pp. 100–104.

[7] J. W. Wallace and M. A. Jensen, "The capacity of MIMO wireless systems with mutual coupling," in *Proc. IEEE Vehicular Technology Conf. (VTC)—Fall*, Vancouver, BC, Canada, 2002, pp. 696–700.

[8] K. Yu and B. Ottersten, "Models for MIMO propagation channels: A review," *Wireless Commun. Mobile Comput.*, vol. 2, no. 7, pp. 653–666, Nov. 2002.

[9] P. Kyritsi and D. Cox, "Effect of element polarization on the capacity of a MIMO system," in *Proc. IEEE Wireless Communications Networking Conf. (WCNC)*, Orlando, FL, 2002, pp. 892–896.

[10] M. J. Gans, N. Amitay, Y. Yeh, H. Xu, R. Valenzuela, T. Sizer, R. Storz, D. Taylor, W. MacDonald, C. Tran, and A. Adamiecki, "BLAST system capacity measurements at 2.44 GHz in suburban outdoor environment," in *IEEE VTS 53rd Vehicular Technology Conf. (VTC)—Spring*, Rhodes, Greece, May 6–9, 2001, vol. 1, pp. 288–292.

[11] N. Chiurtu, B. Rimoldi, and E. Telatar, "Dense multiple antenna systems," in *Proc. IEEE Information Theory Workshop (ITW)*, Cairns, Australia, Sep. 2–7, 2001, pp. 108–109.

[12] A. Moustakas, H. Baranger, L. Balents, A. Sengupta, and S. Simon, "Communication through a diffusive medium: Coherence and capacity," *Science*, vol. 287, no. 5451, pp. 287–290, Jan. 1, 2000.

[13] M. Stoytchev, H. Safar, A. Moustakas, and S. Simon, "Compact antenna arrays for MIMO applications," in *Proc. IEEE Int. Symp. Antennas Propagation Society*, Boston, MA, 2001, vol. 3, pp. 708–711.

[14] J. W. Wallace and M. A. Jensen, "Modeling the indoor MIMO wireless channel," *IEEE Trans. Antennas Propag.*, vol. 50, no. 5, pp. 591–599, May 2002.

[15] R. A. Kennedy, T. D. Abhayapala, and H. M. Jones, "Bounds on the spatial richness of multipath," in *3rd Australian Communications Theory Workshop (AusCTW)*, Canberra, Australia, Feb. 4–5, 2002, pp. 76–80.

[16] M. Fu and L. W. Hanlen, "Capacity of MIMO channels: A volumetric approach," in *Proc. IEEE Int. Conf. Communications (ICC)*, Anchorage, AK, May 11–15, 2003, pp. 2673–2677.

[17] D. A. Miller, "Communicating with waves between volumes: Evaluating orthogonal spatial channels and limits on coupling strengths," *Appl. Opt.*, vol. 39, no. 11, pp. 1681–1699, Apr. 2000.

[18] R. G. Gallager, *Information Theory and Reliable Communication*. New York: Wiley, 1968.

[19] G. Newsam and R. Barakat, "Essential dimension as a well-defined number of degrees of freedom of finite-convolution operators appearing in optics," *J. Opt. Soc. Amer., A*, vol. 2, no. 11, pp. 2040–2045, Nov. 1985.

[20] B. R. Frieden, "Evaluation, design and extrapolation methods for optical signals, based on use of the prolate functions," in *Progress in Optics IX*. Amsterdam, The Netherlands: North Holland, 1971, pp. 311–407.

[21] D. Slepian and H. O. Pollak, "Prolate spheroidal wave functions, Fourier analysis and uncertainty—I," *Bell Syst. Tech. J.*, vol. 40, no. 1, pp. 43–63, Jan. 1961.

[22] C. Flammer, *Spheroidal Wave Functions*. Stanford, CA: Stanford Univ. Press, 1957.

[23] B. Fleury, "First- and second-order characterization of direction dispersion and space selectivity in the radio channel," *IEEE Trans. Inf. Theory*, vol. 46, no. 6, pp. 2027–2044, Sep. 2000.

[24] L. Bayvel and A. Jones, *Electromagnetic Scattering and its Applications*. London, U.K.: Applied Science Publishers Ltd., 1981.

[25] M. Martone, *MultiAntenna Digital Radio Transmission*, ser. Mobile Communications Series. Norwood, MA: Artech House, 2001.

[26] M. J. Gans, "A power-spectral theory of propagation in the mobile-radio environment," *IEEE Trans. Veh. Technol.*, vol. VT-21, no. 1, pp. 27–38, Feb. 1972.

[27] *Microwave Mobile Communication*, W. Jakes, Ed. New York: IEEE Press, 1974.

[28] W. Thompson, *Atlas for Computing Mathematical Functions*. New York: Wiley, 1997.

Leif Hanlen (S'02–M'03) received the bachelor's degrees in electrical engineering, and computer science from the University of Newcastle, Australia, in 1999 and the Ph.D. degree in electrical engineering from the University of Newcastle, Australia, in 2003.

From 1993–1999, he worked with the Electrical Transmission Authority of New South Wales, Australia. He held an assistant teaching position with the University of Newcastle from 2001–2003 and with the Productivity Services Board of Singapore in 2003. Currently, he works as a Researcher with National Information and Communications Technology (ICT) Australia, Canberra, Australia, and serves an adjunct position with the Australian National University. His main research interests include wireless communication systems, information theory, and signal processing.

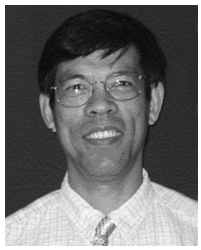

Minyue Fu (S'84–M'87–SM'94–F'04) received the bachelor's degree in electrical engineering from the University of Science and Technology of China, Hefei, China, in 1982, and the M.S. and Ph.D. degrees in electrical engineering from the University of Wisconsin, Madison, in 1983 and 1987, respectively.

From 1983 to 1987, he held a Teaching Assistantship and a Research Assistantship at the University of Wisconsin, Madison. He worked as a Computer Engineering Consultant at Nicolet Instruments, Inc., Madison, WI, in 1987. From 1987 to 1989, he served as an Assistant Professor in the Department of Electrical and Computer Engineering, Wayne State University, Detroit, MI. For the summer of 1989, he was employed by the Universite Catholique de Louvain, Belgium, as a Maitre de Conferences Invited. He joined the Department of Electrical and Computer Engineering, the University of Newcastle, Australia, in 1989. He served as the Head of the Department of Electrical and Computer Engineering from 1998 to 2002. Currently, he is a Chair Professor in Electrical Engineering and the Head of the School of Electrical Engineering and Computer Science. In addition, he was a Visiting Associate Professor at University of Iowa in 1995–1996 and a Senior Fellow/Visiting Professor at Nanyang Technological University, Singapore, 2002. Currently, he is an Area Editor for *Journal of Optimization and Engineering* and Associate Editor for *Automatica*. His main research interests include control systems, signal processing and communications.

Dr. Fu has served as an Associate Editor for the IEEE TRANSACTIONS ON AUTOMATIC CONTROL for 4 years.